

# Moist Internally Cooled Convection

Lokahith Agasthya<sup>1</sup> | Caroline Muller<sup>1</sup> | Mathis  
Cheve<sup>1,2</sup>

<sup>1</sup>Institute of Science and Technology  
Austria, Am Campus 1, 3400  
Klosterneuburg, Austria

<sup>2</sup>École Normale Supérieure de Lyon, 15  
parvis René Descartes, BP 7000, 69342  
Lyon Cedex 07, France

## Correspondence

Lokahith Agasthya, Institute of Science and  
Technology Austria, Am Campus 1, 3400  
Klosterneuburg, Austria  
Email: lnagasthya@gmail.com

## Present address

Institute of Science and Technology Austria,  
Am Campus 1, 3400 Klosterneuburg,  
Austria

## Funding information

European Union Horizon 2020 research  
and innovation programme, Marie  
Skłodowska-Curie grant agreement No.  
101034413; European Research Council  
(ERC), European Union Horizon 2020  
research and innovation programme,  
Project CLUSTER, Grant Agreement No.  
805041

The response of clouds and moist-convective processes to heat-loss to space by long-wave radiative cooling is an important feedback in the earth's atmosphere. It is known that moist convection increases roughly in equilibrium with radiative cooling, an assumption often made in simplified models of the tropical atmosphere. In this study, we use an idealised 2D model of the atmosphere introduced by Vallis et. al. and incorporate a bulk-cooling term which is an idealisation of radiative cooling in the atmosphere. We briefly comment on the static stability of the system to dry and moist convection and characterise its moist convective response to changes in the bulk-cooling. We find that while the clear-sky regions of the model respond directly to the change in the cooling term, the regions dominated by moist convective plumes are insensitive to changes in cooling. Similar to previous findings from Cloud Resolving Models, we too find in our idealised setting that the majority of the increase in convection occurs via an increase in the areal coverage of convection, rather than intensity of convection. We argue that these small-scale convective processes are an upper-bound on how quickly convective intensity can change to stay in equilibrium with radiative cooling.

## KEYWORDS

Moist Convection, Numerical Simulation, Rayleigh-Bénard,  
Radiative Cooling

## 1 | INTRODUCTION

The cooling of the atmosphere by radiative heat-loss to space through outgoing long-wave radiation is one of the most important feedbacks on to global climate. Radiative cooling occurs through a highly interactive, non-linear mechanism with strong vertical and latitudinal variations. Locally, it is strongly dependent on temperature, water vapor content, cloud height and type, the nature of aerosols, partition of water into solid (ice) and liquid phases and several other atmospheric chemical and physical properties. Globally, it is known that the earth is roughly in thermodynamic equilibrium, with the annualised, global mean value of outgoing radiation measured to be  $\sim 1.5 \text{ K d}^{-1}$  [1].

Simplified models of the tropical atmosphere often make the assumption of Radiative Convective Equilibrium (RCE) where the atmosphere is assumed to be in a quasi-equilibrium where moist convection and radiative cooling balance each other over long enough time-scales through convective adjustment [2, 3]. Moist convection is a mechanism by which heat from the earth's surface (heated directly by incoming solar short-wave radiation) is transported upward in the atmosphere in the form of both sensible heat, which is the direct transport of heat by advection, and latent heat, through the transport of water vapour which condenses aloft in the atmosphere. In RCE, these surface fluxes heating the atmosphere are in equilibrium with radiative cooling.

While global climate models are used to understand projected changes in climate and the feedback from various processes on the climate [4], recently Cloud Resolving Models (CRM) have become an important tool to investigate the tropical atmosphere at smaller scale with higher resolution modeling [5]. This approach has gained prominence due to the fact that all GCMs rely on convective parametrisations [6] and are not run at high enough resolutions to resolve convection due to the large computational requirements. Clouds associated with moist convection are known to be a large source of uncertainty in global climate models [7, 8, 9].

CRMs are run over small, often idealised domains typically of the order of a few hundred kilometres in the horizontal direction. CRMs have proved to be extremely successful at providing key and valuable insights into the process of moist convection [10] and also the possible changes in tropical climate with a changing climate characterised by higher surface temperatures [11]. They also allow for the examination of the role of various feedbacks from processes involved in moist convection through sensitivity experiments, where all other feedbacks are held constant while a few are varied in a controlled manner. CRMs usually involve solving equations for a large number of prognostic variables while they also parametrise small-scale processes, in particular parametrisation of sub-grid fluxes and cloud microphysics. It is found often that the choice of such parametrisation can have a significant impact on the resulting dynamics [12]. Further, the large number of parametrised processes and variables make interpretation of results difficult.

In this situation, more theoretical and "blank-slate" simplified studies of moist convection with a few parameters, processes and prognostic variables are valuable. Such an approach can lead to a simplified but still qualitatively accurate representation of convection. In line with this approach are recent studies by Vallis et. al [13], Hernandez et. al [14], Pauluis and Schumacher [15] among others. Here the idea is to represent only the main processes which drive the dynamics of moist convection, which is the release or absorption of heat by the change of phases in water, making their implementation as well as interpretation much more straightforward. Another advantage of simplified models is the vast existing literature on idealised models of dry convection. Rayleigh-Bénard convection is among the best characterised and well-studied natural models [16]. As remarked by Vallis et. al. [13] (henceforth Val2019), there is very little overlap between the study of Rayleigh-Bénard convection and theoretical studies of atmospheric moist convection, particularly of deep convection (i.e. convective clouds that span the whole troposphere).

In the current study, we take forward the model of "Rainy-Bénard" convection from Val2019 and add a uniform, bulk cooling term to mimic atmospheric radiative cooling. We set realistic boundary conditions and fluid parameters,

within the limit of available computational resources, and vary the single value of radiative cooling. We describe and quantify the resulting dynamics, comparing it with known results on the variation of radiative cooling in CRMs.

Notably, Robe and Emanuel [17] found that as the radiative cooling (constant in their idealised CRM experiments) was increased, the convective mass flux showed a roughly linear increase in response. This is expected theoretically, as the subsidence velocity outside clouds is expected to increase proportionally to the radiative cooling. By mass conservation, this implies a similar increase in the upward mass flux in clouds. However, there are no theoretical constraints on how this increased cloud mass flux is reached. This increase could come from either increased mean vertical velocity in clouds, or from increased cloud area. Their numerical simulations showed that most of the convective mass flux increase with strong cooling is due to increased cloud area, while vertical velocities in clouds remain approximately constant.

Here, we first investigate whether our simple model of moist convection correctly captures this behavior found in more complex CRM simulations. Second, we explore whether this can be understood using simple scalings for the vertical velocity in clouds. Importantly, we argue that the small changes in vertical velocities are due to small-scale convective processes, that limit their ability to increase strongly in response to the enhanced radiative cooling.

The rest of the manuscript is organised as follows. Section 2 describes the model and the parameters chosen for the numerical experiments along with a quick summary on the large-scale balances that are expected from the model equations. Section 3 summarises the results of our numerical simulations. Section 3.1 briefly discusses the static stability for the chosen fluid configuration in the presence and absence of moisture and radiative cooling. This is followed by a detailed description of the behaviour of the system for varying the bulk-cooling in Section 3.2. Chiefly, in Section 3.2.1 we examine the scaling of the area fraction of the domain undergoing moist-convection, the vertical velocity and the convective mass-flux with the bulk-radiative cooling. In Sections 3.2.2 - 3.2.4, we propose and examine predictions for the scaling of vertical velocity extremes based on CAPE, buoyancy integrals and cloud-plume models. In Section 3.2.5, we compare the velocity statistics for the moist model with the corresponding dry convective model. We conclude the manuscript in Section 4 with a discussion of our results and avenues for future work.

## 2 | METHODOLOGY

### 2.1 | Model and Equations

Our starting point is the Rainy-Bénard equations of Val2019, with an additional bulk cooling term  $-R$  in the temperature equation, which represents the radiative cooling to space, constant in space and time in our idealised system. We write the equations explicitly in terms of the temperature for a two-dimensional  $(x, z)$  Boussinesq fluid with the buoyancy force proportional to the coefficient of thermal expansion  $\beta$ . The equations for the velocity  $\mathbf{u} = (u, w)$ , the temperature  $T$  and the specific humidity  $q$  (mass of water vapour per unit mass of air) are given by

$$\nabla \cdot \mathbf{u} = 0, \quad (1)$$

$$\partial_t \mathbf{u} + (\mathbf{u} \cdot \nabla) \mathbf{u} = -\nabla p + \nu \nabla^2 \mathbf{u} - \beta T \mathbf{g}, \quad (2)$$

$$\partial_t T + \mathbf{u} \cdot \nabla T + \Gamma_d w = \kappa \nabla^2 T + L_v \tau^{-1} (q - q_s)_+ - R, \quad (3)$$

$$\partial_t q + \mathbf{u} \cdot \nabla q = \kappa_q \nabla^2 q - \tau^{-1} (q - q_s)_+. \quad (4)$$

Here,  $\Gamma_d$  is the dry-adiabatic lapse rate  $g/c_p$  with potential temperature  $\theta$  defined as  $\theta \equiv T + \Gamma_d z$ , where  $\mathbf{g} = (0, g)$

is the amplitude of the acceleration due to gravity,  $c_p$  is the specific heat capacity of dry air at constant pressure.  $q_s$  is the saturation specific humidity of water vapour, which is a function of only temperature in our case. Further,  $L_v$  is the latent heat of condensation of water divided by  $c_p$ ,  $\kappa$  and  $\kappa_q$  are the diffusivity of heat and moisture respectively,  $\nu$  is the kinematic viscosity.  $a_+$  denotes the positive-part of  $a$ , where  $a_+ = 0$  when  $a$  is negative and  $a_+ = a$  when  $a$  is positive.  $\tau$  is a time-scale of condensation, which is set to be very small so that condensation is almost instantaneous whenever the specific humidity of water vapour  $q > q_s$ . Note that condensates are assumed to precipitate instantaneously, so there are no suspended condensates (no sustained clouds) in our simulations.

In this system,  $q$  is assumed to always be small such that virtual effects arising from the presence of water vapour are neglected. Thus, the changes in density and heat-capacity of air due to water vapour are not included in the model. The simplified Clausius-Clapeyron equation for the saturation specific humidity of water vapour in the model is given by [13]

$$q_s(T) = q_0 \exp \alpha(T - T_0), \quad (5)$$

where  $T_0 = 300$  K, with  $q_0$  being the saturation specific humidity at  $T = T_0$ .

It remains to specify the boundary conditions for the system. The domain is periodic in the horizontal direction. The temperature and specific humidity are kept constant at the top and bottom boundaries while the fluid is held motionless. The values are

$$\mathbf{u}(z = 0) = \mathbf{u}(z = 10 \text{ km}) = \mathbf{0}; \quad (6)$$

$$T(z = 0) = 300 \text{ K}; \quad (7)$$

$$T(z = 10 \text{ km}) = 230 \text{ K}; \quad (8)$$

$$q(z = 0) = 0.8q_s(300 \text{ K}) = 0.02 \text{ kg kg}^{-1}; \quad (9)$$

$$q(z = 10 \text{ km}) = 0.1q_s(230 \text{ K}) = 5.26 \times 10^{-5} \text{ kg kg}^{-1}. \quad (10)$$

The bottom and top surface are held at a constant relative humidity of 80% and 10% respectively. Henceforth, we denote as  $T_{bot}$  and  $q_{bot}$  the set temperature and specific humidity at the lower boundary and  $T_{top}$  and  $q_{top}$  for the same quantities at the top boundary. The temperature difference between the lower surface and the upper surface is 70 K, which is smaller than the "dry adiabatic" value 100 K - the underlying dry system is thus stable to dry convection.

The equations are written here in terms of the temperature  $T$  rather than buoyancy  $b$  (as in Val2019) and with changes in density expressed in change in  $T$  assumed to be proportional to the expansion coefficient  $\beta$ . The choice of using temperature is to help readers to make direct comparisons with dimensional, atmospheric values. Dynamically, these equations are identical to the equations in Val2019, except for the bulk-cooling term, which is the main focus of our study.

We solve the adimensionalised equations (equations (1)-(4)) with length, time and temperature normalised by 1 km, 1 hr and 1 K respectively. The equations are solved in python using the Initial Value Problem (IVP) command from the Dedalus package [18]. Dedalus provides an open-source framework for solving differential equations by spectral decomposition. The equations are solved by decomposition into spectral bases, using Fourier bases for the horizontal direction and Chebyshev polynomial bases for the vertical direction. Dedalus allows the user to simply input differential equations as strings, allowing for quick and easy code-development.

Table 1 summarises the parameters and scales used in the simulations. The simulation corresponds to a domain 100 km wide and 10 km high. Values of temperature, specific humidity and the saturation specific humidity are realistic.

Quantity	Value in Simulation	Physical Units	Typical Atmospheric Value
Length	1	1 km	-
Time	1	1 h	-
Temperature	1	1 K	-
$\kappa$	0.004	$1.1 \text{ m}^2 \text{ s}^{-1}$	$\sim 2 \times 10^{-5} \text{ m}^2 \text{ s}^{-1}$
$\nu$	0.0028	$0.77 \text{ m}^2 \text{ s}^{-1}$	$\sim 1.5 \times 10^{-5} \text{ m}^2 \text{ s}^{-1}$
$\kappa_q$	0.0052	$1.43 \text{ m}^2 \text{ s}^{-1}$	$\sim 2.6 \times 10^{-5} \text{ m}^2 \text{ s}^{-1}$
$\beta g$	1	$7.5 \times 10^{-5} \text{ m s}^{-2} \text{ K}^{-1}$	$\sim 0.03 \text{ m s}^{-2} \text{ K}^{-1}$
$\Gamma_d = g/c_p$	10	$10 \text{ K km}^{-1}$	$10 \text{ K km}^{-1}$
$L_v/c_p$	2500	2500 K	$\sim 2500 \text{ K}$
$q_0$	0.025	$0.025 \text{ kg kg}^{-1}$	$0.025 \text{ kg kg}^{-1}$
$\alpha$	0.05516	$0.05516 \text{ K}^{-1}$	$\sim 0.055 \text{ K}^{-1}$
$R$	[0 – 0.3]	[0 – 7.2] $\text{K d}^{-1}$	[1 – 2] $\text{K d}^{-1}$

**TABLE 1** Parameters used for simulations of moist internally cooled convection with varying  $R$ , solved using Dedalus on a  $100 \text{ km} \times 10 \text{ km}$  domain and a  $2048 \times 256$  grid. We set  $T_{bot} = 300 \text{ K}$ ,  $T_{top} = 230 \text{ K}$ ,  $q_{bot} = 0.8q_s(T_{bot})$  and  $q_{top} = 0.1q_s(T_{top})$ . In other simulations,  $\kappa$ ,  $\beta g$  and the boundary conditions are varied and the chosen parameters are stated clearly in the text describing the results.

We set large values for the dissipation constants  $\kappa$ ,  $\nu$  and  $\kappa_q$ , while keeping their ratios realistic. That is, the non-dimensional constants of viscous forces, the Prandtl number  $\text{Pr} = \nu/\kappa$  and the water vapour Prandtl number  $\text{Pr}_q = \kappa_q/\kappa$  are both set to their dry air values of 0.7 and 1.3 respectively. Thus, we are simulating an atmosphere where the viscous, dissipative forces are far larger in magnitude and the buoyancy force ( $\beta g$ ) is weaker than in reality. Decreasing the dissipation constants would require a far higher resolution numerical grid and much greater computational resources to have a well-resolved energy-cascade in the absence of any sub-grid scale parametrisations.

The time-scale of condensation  $\tau$  is set small enough to ensure that large regions of supersaturation (i.e. with relative humidity larger than 100%) do not develop anywhere in the domain, with the maximum relative humidity attained staying below 1.02. This ensures that all simulations are in the regime of instantaneous condensation and precipitation. For the largest value of  $R = 7.2 \text{ K d}^{-1}$ , this corresponds to  $\tau = 0.36 \text{ s}$  or  $1 \times 10^{-4}$  in simulation units. For smaller values of  $R$ ,  $\tau$  is increased appropriately to have faster simulation wall-time. We have checked via shorter runs that the precise value of  $\tau$  chosen does not affect the main results as long as the simulation remains in the regime of instantaneous condensation.

## 2.2 | Large-scale energy balance

For a system in thermal equilibrium, the sum of the sensible heat flux and the latent heat-flux into the system from the boundaries must balance the net radiative cooling in the domain. This is expressed as

$$\frac{\kappa}{L_z} \left( \partial_z \bar{T} \Big|_{z=L_z} - \partial_z \bar{T} \Big|_{z=0} \right) + L_v \frac{\kappa q}{L_z} \left( \partial_z \bar{q} \Big|_{z=L_z} - \partial_z \bar{q} \Big|_{z=0} \right) = R. \quad (11)$$

The above equation is derived by first summing equation (3) and equation (4) multiplied by  $L_v$  and then considering the domain average of the resulting equation in the steady-state (overbars denote horizontal and time averages). Time and horizontal derivatives vanish due to the steady-state condition and the periodic boundary conditions respectively. Since  $w = 0$  at the top and bottom boundaries, the domain average only depends on the vertical gradients of the temperature and specific humidity evaluated at these boundaries.

The four terms on the LHS of eqn. (11) are the sensible heat flux into the domain from the top and bottom boundaries and the latent-heat flux from the top and bottom boundaries respectively. The four terms summing up to  $R$  is a check that the simulations are in thermal equilibrium. The height-wise heat-transfer can be deduced by considering only the horizontal average of the sum of equation (3) and  $L_v$  times equation (4). An integration in the variable  $z$  between  $z$  and  $L_z$  gives

$$\overline{w(T + L_v q)} - \partial_z (\kappa \bar{T} + L_v \kappa q \bar{q}) = R(L_z - z) + C_0. \quad (12)$$

Here again, the overbar indicates the time and horizontal average at a given height  $z$ , and  $C_0$  is a constant of integration equal to (minus) the sum of the outgoing latent and sensible heat flux at the top boundary ( $C_0 = -\partial_z (\kappa \bar{T} + L_v \kappa q \bar{q}) \Big|_{z=L_z}$ ). The first two terms on the LHS are the convective transport of sensible heat and latent heat respectively while the latter two terms represent the conductive transport of sensible heat and latent heat. The sum of these is thus a straight-line in  $z$  with slope  $-R$ . The convective transport terms show large variations in time and equation (12) is not satisfied at any instantaneous time. Statistically, however, equation (12) is satisfied in our simulations, which is essential to ensure that the statistics measured in the study represent the true long-term, steady-state behaviour and not a transient solution.

## 3 | RESULTS

### 3.1 | Conditional Stability

For the temperature boundary-conditions chosen, the dry system ( $q = 0$ ) with no radiative cooling ( $R = 0$ ) is stable to small perturbations, as the steady state solution ( $u = 0, \kappa \nabla^2 T = 0 \Rightarrow T(z) = (T_{top} - T_{bot})z/L_z + T_{bot}$ ) has a linear temperature profile with a gradient of  $7 \text{ K km}^{-1}$  that is less steep than the adiabatic lapse rate of  $10 \text{ K km}^{-1}$ . In the presence of moisture, the static stability is determined by a combination of the moisture and temperature boundary-conditions. While the steady-state solution ( $q(z) = (q_{top} - q_{bot})z/L_z + q_{bot}$ ) is given by a linear decrease of  $q$  with height,  $q_s$  decreases much faster (exponentially) with height, with condensation likely to trigger convection in the system. The steady-state solution where condensation occurs without convection and the latent-heat is balanced exclusively by thermal dissipation is discussed by Val2019 (Section 5, "The drizzle solution"). When  $R$  is non-zero, the steady-state solution depends on  $R$  - the variation of this solution with  $R$  and its linear stability are not considered in this study.

For the chosen  $q_{bot}$  and  $q_{top}$ , the system is unstable and shows moist convection even with  $R = 0$ . The convection is not steady in time - instead, it is interspersed by long time periods during which the fluid is quiescent and the

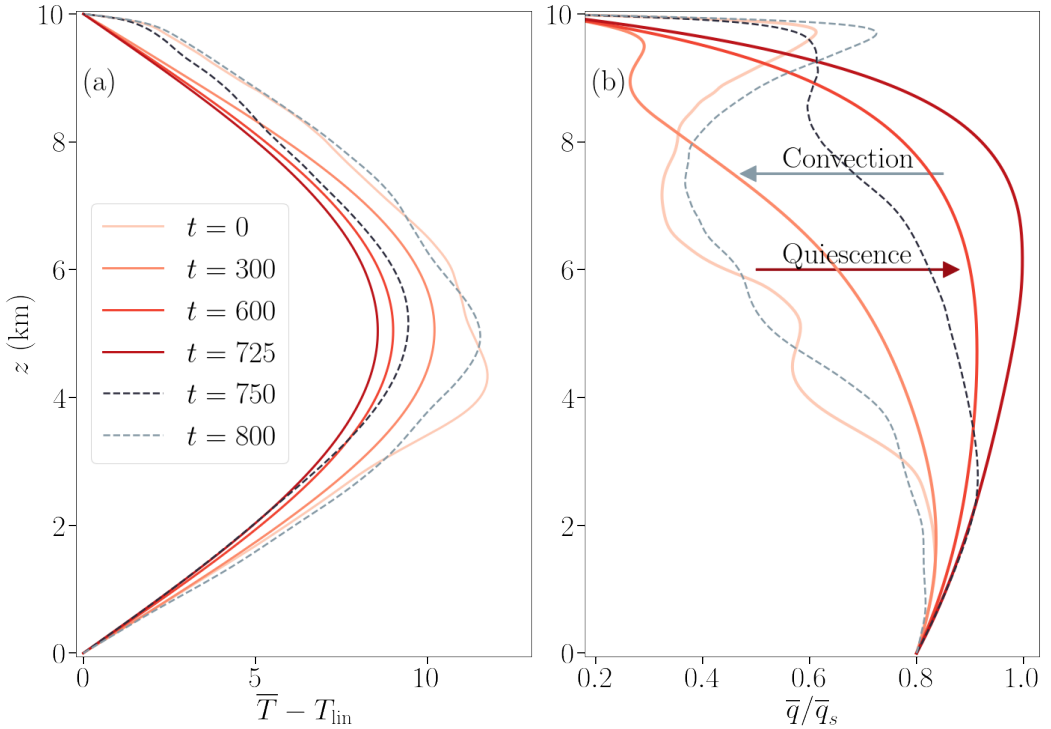


**FIGURE 1** The temperature and relative humidity profiles for the moist simulations with  $R = 0$ . (a) The anomaly of the horizontally averaged temperature profile  $\bar{T}$  with respect to the linear temperature profile  $T_{lin} = (T_{top} - T_{bot})z/L_z + T_{bot}$  for different times. (b) Average relative humidity profile  $\bar{q}/\bar{q}_s$  for different times.

temperature gradually decreases while the quantity of moisture in the domain increases, both quantities relaxing towards a linear profile. Thus, the relative humidity  $q/q_s$  increases through both, an increase in  $q$  and a decrease in  $q_s$ . When the domain reaches saturation in some regions, it leads to local condensation and convection which quickly becomes space-filling. Rapid convective adjustment brings the system back to a quiescent warm, dry state through condensation and latent heating and the process repeats cyclically. Figure 1, showing the average temperature and relative humidity profiles at different times, summarises this behaviour. Initially at  $t = 0$  (light red, solid curve), the temperature is warm in the bulk and the relative humidity is well below 1 everywhere. The temperature slowly shifts towards the linear profile (darker shades of red) until around  $t = 725$ , where  $q/q_s$  between  $z \sim 6$  and  $z \sim 8$  is very close to 1. Condensation occurs here, heating up the system and causing the temperature to once again gain a strong positive anomaly with respect to the linear profile (blue dashed curves) with the domain becoming drier. At  $t = 800$  (light, blue dashed curve), the system is again where it was at  $t = 0$  (light, red dashed curve) and returns to a quiescent state. Supplementary Movie 1 shows an animation of the relative-humidity field (top panel) and the profiles of  $T$  (bottom left panel),  $q$  and  $q_s$  (bottom right panel).

For  $R > 0$ , the dry steady-state solution ( $\mathbf{u} = \mathbf{0}$ ) is given by a parabolic temperature profile in  $z$  such that  $\partial_z^2 T = R/\kappa$ , which can be solved analytically for the fixed temperature boundary conditions. The static stability of the solution can be ascertained by checking if  $\partial_z T < -10 \text{ K km}^{-1}$  everywhere. In our case, static stability holds everywhere for  $R < 5.76 \times 10^{-2} \text{ K d}^{-1}$ . Thus, even a small magnitude of radiative cooling alone destabilises the fluid layer and leads to dry convection. The precise small value of  $R$  for which the moist convection changes from intermittent to continuous has not been explored in this study. Instead, we focus on the response of moist convection to varying radiative cooling rates, which we discuss next.

### 3.2 | Varying Radiative Cooling

In the rest of the paper, we focus on the behaviour of the system for 5 non-zero values of radiative cooling,  $R = 0.72 \text{ K d}^{-1}$ ,  $1.5 \text{ K d}^{-1}$ ,  $2 \text{ K d}^{-1}$ ,  $3.6 \text{ K d}^{-1}$  and  $7.2 \text{ K d}^{-1}$ , varying the magnitude of  $R$  by a factor of 10. The boundary conditions and all other fluid parameters are kept fixed, while  $R$  is varied. When  $R$  is increased, the domain is cooled in the bulk and the average domain temperature decreases. Due to the decreased temperature, there is also lesser moisture in the domain, as  $q_s$  decreases with  $T$  and any moisture beyond the saturation specific humidity is rapidly removed by condensation.

Figure 2 shows instantaneous snapshots of the relative humidity ( $q/q_s$ ) for two flows with  $R = 1.5 \text{ K d}^{-1}$  (top panel) and  $R = 3.6 \text{ K d}^{-1}$  (lower panel). The two snapshots are shown for the instant at which the largest vertical velocity  $w$  is realised throughout the run. It is apparent from the snapshots that the flows with larger  $R$  have a much larger area undergoing convection. This can be seen by comparing the fraction of the domain occupied by the contours of 98% relative humidity. While there are no real clouds in the simulation, i.e., we do not track condensed liquid water, it is still possible to study cloudy dynamics by considering "clouds" as grid points which are supersaturated, i.e. where the condensation term in equation (3) is non-zero. Due to the sharp discontinuity of this term, we henceforth define clouds as grid points with  $q/q_s > 0.98$ . While our analysis and results remain virtually unchanged if we include only super-saturated points, having a slightly lower RH threshold gives greater cloud statistics.

We now recall the theoretical expectations for the response of a moist convecting atmosphere to increased radiative cooling. As mentioned in the introduction, in clouds the total upward mass flux  $M_c$  is expected to increase linearly with radiative cooling. Indeed, in the concluding remarks of the work by Robe and Emanuel [17], the authors point out that "The net upward mass flux carried by moist convection is strongly constrained by the requirement that the subsidence warming outside of the active condensation balance the radiative cooling". For a Boussinesq fluid with



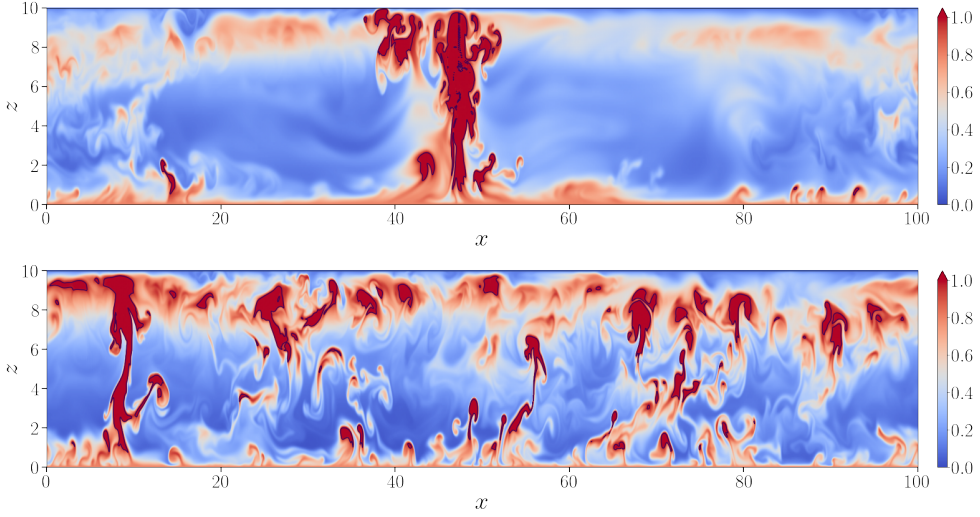


**FIGURE 2** Instantaneous snapshots of the relative humidity ( $q/q_s$ ) for two simulations with  $R = 1.5 \text{ K d}^{-1}$  (top panel) and  $R = 3.6 \text{ K d}^{-1}$ . The snapshots are taken at the time with the largest  $w$  value of the whole run. Black solid lines represent clouds, ie., contours of  $q/q_s = 0.98$ .

constant density, the mass flux per cloud is simply proportional to the average upward velocity in clouds, which we denote  $w_c$ . If we denote  $\sigma$  the area fraction of cloudy grid points at a given height, mass conservation yields

$$M_c = \sigma w_c = (1 - \sigma) w_{sub}, \quad (13)$$

where  $M_c$  is the cloudy upward mass flux, and  $w_{sub}$  is the average downward vertical velocity outside clouds. The crux of the Robe and Emanuel's statement is that since  $w_{sub}$  is unaffected by condensation, it must depend only on the radiative cooling. This can be seen by considering equation (3) outside clouds. Far away from the vertical boundaries, we can neglect diffusion and assuming that horizontal advection is small, the time and horizontal average of equation (3) over the subsiding region gives

$$\langle w(\Gamma_d + \partial_z T) \rangle_{sub} \sim -R, \quad (14)$$

where  $\langle \rangle_{sub}$  indicates the average over the clear-sky regions. For the average velocity  $w_{sub}$  outside clouds we have

$$w_{sub}(\Gamma_d - \Gamma_m) \sim R, \quad (15)$$

where  $\Gamma_m = -\partial_z T_{sub}$  is some typical (moist) value of the lapse rate of the domain outside clouds, which is meant to represent the moist adiabatic lapse rate in clouds. Indeed, moist convection in clouds is expected to bring the whole

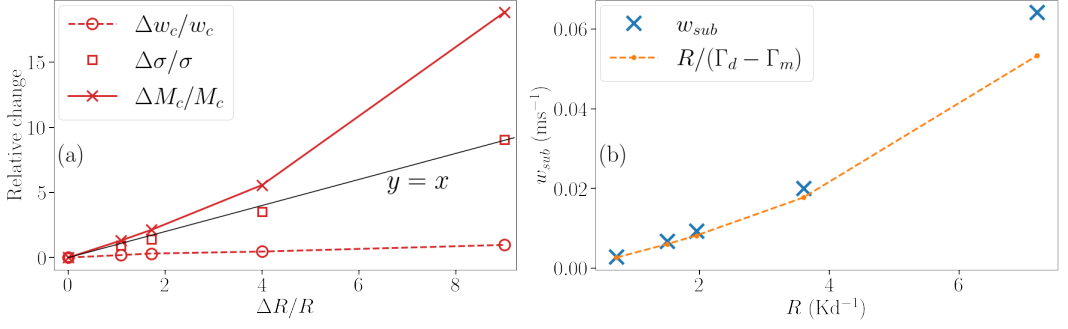


**FIGURE 3** (a) The relative change in the Cloud Volume Fraction  $\sigma$ , the time-averaged vertical velocity in clouds  $w_c$  and the convective upward mass flux  $M_c$  measured at  $z = 4.5$  km. The  $y = x$  line is shown for reference. (b) Average measured downward velocity outside clouds  $w_{sub}$  compared with a descent in equilibrium with radiation and the lapse rate equal to  $\Gamma_m$  (see equation (15)) at  $z = 4.5$  km. Here for  $\Gamma_m$  we use the theoretical moist adiabatic lapse rate for the domain average temperature measured in the simulation from equation (18).

atmosphere towards this moist adiabatic lapse rate with the weak horizontal temperature gradients in the tropics implying that this lapse rate is imprinted over the whole domain (by gravity waves [19]). Thus the lapse rate outside clouds is expected to match the moist adiabatic lapse rate in clouds. Combining equations (13) and (15) yields

$$M_c = \sigma w_c \sim (1 - \sigma)R/(\Gamma_d - \Gamma_m). \quad (16)$$

If we assume that  $\Gamma_m$  remains fixed with  $R$  and  $\sigma \ll 1$ , this gives  $M_c \sim R$ , which is the oft repeated statement that the cloudy mass flux increases in equilibrium with  $R$ .

### 3.2.1 | Scaling of Convective Mass Flux

The above theoretical constraints on the total mass flux in clouds  $M_c = \sigma w_c$  do not predict whether the upward mass flux increases due to an increase in the intensity of convection and faster updraughts (greater  $w_c$ ) or through an increase in the amount of convection that occurs at a given time (greater  $\sigma$ ) or a combination of the two effects. As mentioned in the introduction, simulations in Cloud Resolving Models [17] have found that an increase in  $R$  leads to a large relative increase in  $\sigma$  while  $w_c$  remains nearly fixed even for large variations in the magnitude of the imposed cooling.

Qualitatively, Figure 2 seems to indicate larger cloud fraction with stronger radiation in our simple model as well. We quantify the variation in  $w_c$ ,  $\sigma$  and  $M_c$  for increasing  $R$  by measuring their individual relative changes, relative to their value in the simulation with the smallest  $R$  of  $R_0 = 0.72 \text{ K d}^{-1}$ . This is written as

$$\Delta \sigma/\sigma = \frac{\sigma(R) - \sigma(R_0)}{\sigma(R_0)} \quad (17)$$

and similarly for  $w_c$  and  $M_c$ . The relative changes at height  $z = 4.5$  km are shown in panel (a) of Figure 3. This

height corresponds to a strongly convective zone where  $w_c$  is close to its maximum value in the vertical while  $\sigma$  is increasing with height. Analogous to the height selected by Robe and Emanuel [17] for their analysis, we consider this height as representative of the convective strength, since vertical velocities are near their maximum magnitude and strong entrainment has not yet commenced.

Figure 3(a) shows that the cloudy area fraction increases linearly with  $R$ , with a ten-fold increase in  $R$  (or  $\Delta R/R = 9$ ) leading to a ten-fold increase in  $\sigma$ .  $w_c$  shows only a small change in magnitude, approximately doubling for the ten-fold increase in  $R$  while the convective mass flux  $M_c$  shows a super-linear increase. It is clear that the bulk of the contribution to the increased mass-flux comes from the large increase in the cloudy area fraction, consistent with previous results from CRMs. Panel (b) of the same figure shows the variation of  $w_{sub}$  with  $R$  at the same height in the domain. The relative change in  $w_{sub}$  is  $> 20$ , showing that the subsidence velocity increases far faster than the increase in magnitude of  $R$ . We compare the subsidence velocity with the theoretical estimate from equation (15), with  $\Gamma_m$  taken to be the moist adiabatic lapse rate given by (see equation (3.4) of Val2019)

$$\Gamma_m = \frac{\Gamma_d}{1 + L_v \alpha q_s(\bar{T})}, \quad (18)$$

where  $\bar{T}$  is the measured horizontal average temperature at a given height. We emphasise here that the measured lapse-rate  $-d\bar{T}/dz$  in the domain differs slightly from the theoretical moist-adiabatic lapse-rate  $\Gamma_m$  - the measured value is about  $1 \text{ K km}^{-1}$  steeper than  $\Gamma_m$  in all simulations - leading to an overestimate for  $w_{sub}$ .

This discrepancy comes from the fact that the average measured  $w_{sub}$  hides the significant spatial variability in vertical velocity over the domain while the theoretical estimates rely on the idealised assumption of a uniformly subsiding dry region outside clouds with perfectly coherent rising moist plumes within clouds. This small quantitative mismatch is interesting and deserves further investigation, but is beyond the scope of this study. For our purpose, it is sufficient to understand  $(\Gamma_d - \Gamma_m)$  as just a multiplying lapse-rate scale for  $w_{sub}$  so the product scales as  $R$ . Note that  $w_{sub}$  itself thus scales approximately with  $R$  (Figure 3b), though not exactly. The value of  $\Gamma_m$  increases with  $R$  (moist-adiabatic lapse rate becomes less steep) due to the decrease in temperature at a given height - larger  $R$  leads to a colder domain, leading to a decrease in  $q_s$  and thus a moist lapse-rate that is closer to the dry lapse-rate.

So it is clear that in the moist-convective system, the subsidence velocity outside clouds is set by a combination of  $R$  and the response of the temperature field to  $R$ . A ten-fold increase in  $R$  also leads to a halving of  $(\Gamma_d - \Gamma_m)$  (or a doubling of the  $(\Gamma_d - \Gamma_m)^{-1}$ ), which explains the large increase of  $w_{sub}$ . The subsidence velocity is thus sensitive directly to  $R$  and is also influenced by the changing lapse-rate, which is an indirect effect of changing  $R$ . In summary, our results show that, consistent with theory and CRM simulations, the subsidence velocity scales approximately linearly with the radiative cooling amplitude, albeit a slight change in the proportionality factor due to changes in the moist adiabatic lapse rate. As a consequence, the total cloud mass flux increases linearly with the radiative cooling amplitude, largely due to increased cloud fraction, while the average velocity in clouds remains largely insensitive to the radiative cooling rate. The small change over a large range of parameters is an indication that the convective velocity scale is likely set by small-scale, convective processes alone, a hypothesis that we further investigate next.

### 3.2.2 | Vertical Velocity

The simple model of moist convection under current investigation correctly captures the variation in the cloudy mass flux with changing  $R$ , as results from previous work with CRMs has shown. The vertical velocity in the model as yet remains unconstrained and it still remains unclear what sets the updraught velocities. We investigate the velocity

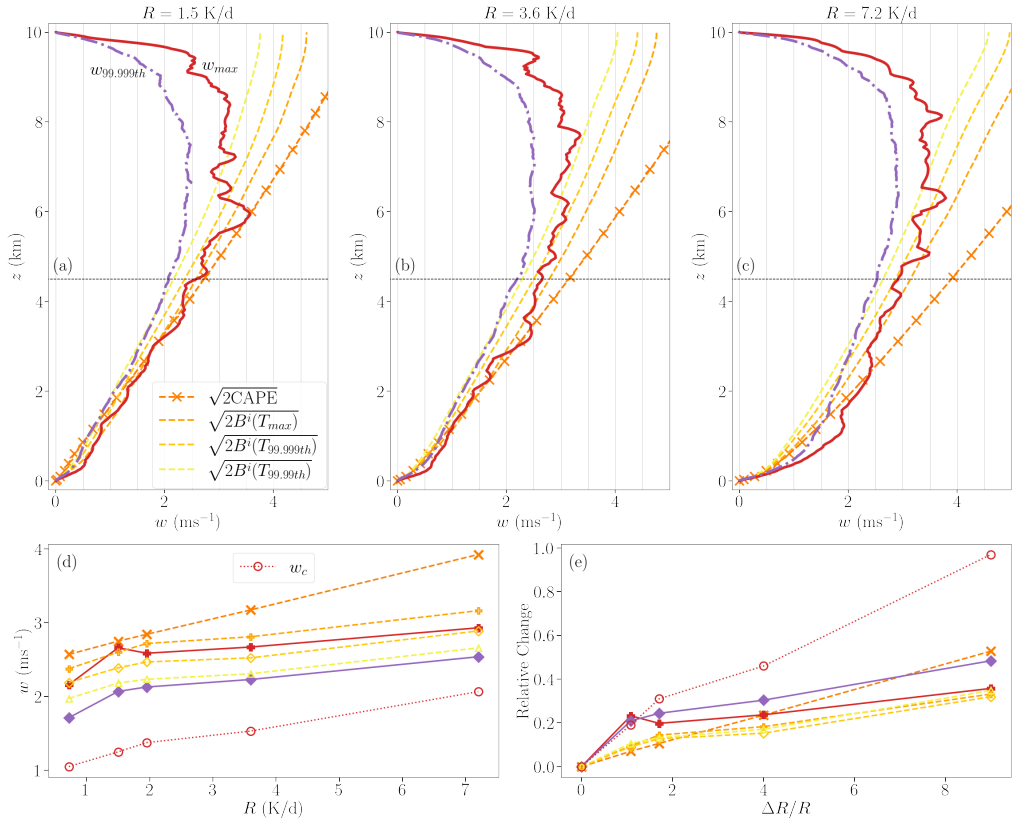


**FIGURE 4** Maximum vertical velocity  $w_{max}$  (red solid line) and the 99.999th percentile vertical velocity  $w_{99.999th}$  (purple dotted line) at each height for (a)  $R = 1.5 \text{ K d}^{-1}$ , (b)  $R = 3.6 \text{ K d}^{-1}$  and (c)  $R = 7.2 \text{ K d}^{-1}$ . This is compared with the velocity predicted by the buoyancy integral of the maximum, 99.999th and 99.99th percentile of temperature, (yellow dashed lines) and CAPE (orange crosses). Panels (d) and (e) show the values of the same quantities and their relative change respectively at  $z = 4.5$  km, indicated by a horizontal dashed line in the upper panels, addition to the average velocity in clouds  $w_c$ .

extremes and the distribution of the vertical velocity in the domain for different  $R$ . In all the simulations, the median vertical velocity is slightly negative, with greater than half of the domain being occupied by subsiding flows ( $w < 0$ ). The up-down asymmetry is consistent with previous studies of dry stratified convection [20, 21], with the  $-R$  term breaking the up-down symmetry. Further, the presence of moisture and condensation without evaporation in the model also leads to latent heating of rising parcels of fluids, without a corresponding evaporative cooling of subsiding parcels. This asymmetry exists in more complex models as well as in the true atmosphere, due to the fact that some of the condensates precipitate during ascent, and are thus not present to evaporate during descent.

Convective available potential energy (CAPE) is an important measure used to characterise the instability of a column of moist air. CAPE is a vertical buoyancy integral calculated relative to a domain mean, where an idealised parcel is assumed to rise first dry-adiabatically ( $\partial_z T = -\Gamma_d$ ), conserving its moisture content until it becomes saturated (ie., reaches the dew point), following which the ascent is assumed to be moist-adiabatic ( $\partial_z T = -\Gamma_m$ , see equation (??)). CAPE is used to estimate the maximum kinetic energy such an idealised parcel can attain due to buoyancy-lifting. In general, for a parcel ascent which follows a given rising parcel temperature profile  $T_p(z)$ , the buoyancy integral  $B^i(T_p)$  up to a height  $z$  is given by

$$B^i(T_p) = \beta g \int_0^z (T_p(z) - \bar{T}(z)). \quad (19)$$

The buoyancy integral leads to a prediction of vertical velocity given by  $\sqrt{2B^i}$  for a parcel with temperature  $T_p$  lifted through a background temperature profile  $\bar{T}$ . While CAPE, calculated using the moist-adiabatic ascent, is commonly calculated for atmospheric soundings and to predict the intensity of impending thunderstorms, Singh and O'Gorman [22] found a closer correlation between the buoyancy integral of temperature extremes and the maximum velocity in CRM simulations  $B^i(T_{extreme})$ .

Here, we compare the 99.999th percentile ( $w_{99.999th}$ ) as well as the maximum vertical velocity ( $w_{max}$ ) at each height to CAPE and the buoyancy integral velocity of the 99.99th percentile, 99.999th percentile and the maximum temperature attained at each height during the runs. The upper panels of Figure 4 show  $w_{max}$  and  $w_{99.999th}$  for three values of  $R$  - the maximum  $w$  (red) remain remarkably similar even for large variations in  $R$  while the 99.999th percentile of  $w$  (purple) shows a small shift towards the right. These represent the most rapidly rising thermal plumes, with the fastest rising parcels without exception lying inside clouds. Even as the cloudy mass flux and the average downward velocity of the compensating subsiding flow outside clouds both increase by an order of 20, the maximum velocity in clouds as well as the average velocity in clouds remain stubbornly fixed independent of  $R$ . Zooming out momentarily, we found that the maximum vertical velocity at any height attained in the domain stays strictly between  $3.2 \text{ m s}^{-1}$  and  $3.9 \text{ m s}^{-1}$  even when  $T_{bot}$  is raised to 302.5 K, decreased to 297.5 K, when  $T_{top}$  is increased or decreased by up to 15 K and even when  $\kappa$  is halved, for various imposed values of  $R$  (a detailed study of the dynamics of the model for varying parameters other than  $R$  is not taken up in the current study). However, when  $\beta g$  was increased by a factor of 5, an approximate doubling of  $w_{max}$  was seen, indicating that  $w_{max}$  is most closely related to the buoyancy integrals and the mechanism that sets the temperature anomaly of the cloudy rising plumes.

Figure 4 also shows the vertical velocity predicted by CAPE as well as the buoyancy integrals of the highest percentiles of  $T$ . CAPE (orange crosses) seems like an excellent prediction for  $w_{max}$  for  $R = 1.5 \text{ K d}^{-1}$ , as seen in panel (a). This result however is not robust when  $R$  is varied, as shown in panels (b) and (c), CAPE is a large overestimation of the vertical velocity. The buoyancy integrals of the temperature extremes (going from yellow to orange) predict the highest velocity percentiles extremely well, up to  $z \sim 6 \text{ km}$ . The departure of the temperature extremes from the domain average temperatures (not shown) are also independent of  $R$ . Panel (d) shows the values of  $w_{max}$ ,  $w_{99.999th}$

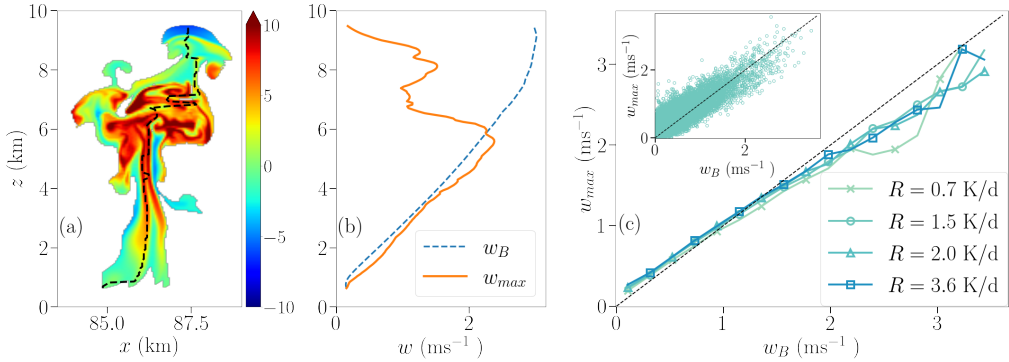


**FIGURE 5** (a) Temperature anomaly with respect to domain and time-average horizontal mean in a chosen cloud plume. The boundary of the cloud is the contour of 98% relative humidity and the black dashed line shows the location of the maximum  $w$  within the cloud at a given height. (b) The maximum velocity  $w_{max}$  at each height for the cloud plume in panel (a) compared with the predicted vertical velocity  $w_B$  from the buoyancy integral. (c) Inset shows the scatter plot of  $w_B$  and  $w_{max}$  within the cloud for all clouds in the simulation with  $R = 1.5 \text{ K d}^{-1}$  with  $w_0, \mathcal{B} > 0$ . The main figure in panel (c) shows the same horizontally binned average of the same scatter plot for other values of  $R$ . The dashed line represents the  $y = x$  line.

and the buoyancy integral velocities at  $z = 4.5 \text{ km}$  as a function of  $R$ , while panel (e) shows the relative change of these quantities as a function of the relative change in  $R$ . CAPE at a fixed height increases linearly with increasing  $R$  - the increase is due to the fact that the domain on average becomes colder while the temperature of a moist adiabatic ascent remains fixed for the same boundary conditions. The magnitude of buoyancy integral velocities follow the extreme vertical velocities closely, with the 99.99th percentile of temperature (yellow) being an excellent predictor of the 99.999th percentile of  $w$  (purple). We also show the average velocity in clouds  $w_c$  for readers to make a comparison with Figure 3(a) while noting the change in the y-axis range.

The extreme velocities show a small increase ( $\sim 50\%$ ) over the parameter range, which is broadly similar to the growth in buoyancy integrals and in CAPE. However, the majority of this increase comes in going from  $R = 0.7 \text{ K d}^{-1}$  to  $R = 1.5 \text{ K d}^{-1}$ , following which the extreme velocities remain nearly constant while CAPE continues to grow linearly. It is important to note here that even if  $w_{max}$  grew similar to the CAPE velocity, the relative increase is still very small compared to the increase in  $\sigma$  and  $M_c$  discussed in the previous section. Importantly, regardless of the buoyancy estimate used to predict  $w$  changes, these integrals are constraints on vertical velocity, preventing its strong increase with  $R$ , and are responsible for the fact that the increased mass flux is almost entirely achieved through increased cloud fraction.

### 3.2.3 | Velocity in individual clouds

In the previous section, we considered buoyancy integrals of the temperature extrema from the entire simulation run and found that these integrals scale very closely with the extrema of vertical velocities from the simulation. While this gives us cause for cautious optimism, it must be noted that the profile of maximum or 99.999th percentile of temperature does not exactly correspond to any single instant in the simulation. Here, we exploit the simplicity of our idealised set-up to investigate individual clouds to find the correlation between the maximum velocity within a cloud plume with the buoyancy integral of this cloud. Noting that the horizontally averaged temperature profile  $\bar{T}$

shows little variation in time, we measure the buoyancy integral for individual clouds from the maximum temperature attained at each height in the cloud. At leading order, the balance between the advection term and the buoyancy term in the vertical component of the momentum equation (2) leads to

$$w \partial_z w \approx \beta g (T(z) - \bar{T}) \implies \frac{1}{2} (w(z)^2 - w(z_0)^2) \approx \beta g \times \int_{z_0}^z (T(z) - \bar{T}(z)) dz, \quad (20)$$

where  $z_0$  is the height of the cloud-base. Then, in a given cloud, the parcel with the fastest vertical speed of ascent  $w_B$  should correspond to an upward moving parcel which begins at  $z_0$  with vertical velocity  $w_0$  and accelerating at a rate predicted by the buoyancy integral calculated with respect to the maximum temperature in the cloud at the given height. This leads to

$$\max_x (w(z)) \approx w_B(z) \equiv \sqrt{w_0^2 + 2\mathcal{B}(z)} \quad \text{with} \quad \mathcal{B}(z) = \beta g \times \int_{z_0}^z \max_x (T(z) - \bar{T}(z)) dz \quad (21)$$

where  $\max_x f$  is the maximum of the function  $f$  at a fixed height within the given cloud. Thus,  $w_B$  is a prediction for the maximum velocity inside a cloud given a profile of the maximum temperature inside the same cloud.

Panel (a) of Figure 5 shows the snapshot of the temperature anomaly of a single "well-behaved" cloud from the simulation with  $R = 1.5 \text{ K d}^{-1}$ , with the location of the vertical velocity maximum corresponding well with the regions shaded with the deepest red colour (warmest). A cloud is defined as a contiguous region with  $q/q_s > 0.98$  as in the rest of the study. Clouds were identified using the 'skimage.measure.regionprops' function of the scikit-image python package [23]. Panel (b) shows the maximum vertical velocity at each height within the cloud, compared with the prediction  $w_B$  from equation (21). We see that the predicted  $w_B$  matches the measured  $w_{max}$  excellently up to about the height at which the cloud  $w_{max}$  profile reaches its maximum value in  $z$ . The horizontal location of the  $w$  maximum in the cloud (indicated by the black, dashed line in panel (a)) also indicates that this corresponds to a single, vertically rising warm parcel. Above this height, which we denote  $z_{max}$ ,  $w_{max}$  falls off as the plume does not remain as coherent and the temperature anomaly of the cloud decreases due to combination of adiabatic cooling of the fast-rising parcel, the decrease in moisture content due to condensation and turbulent entrainment of non-cloudy air at the edge of clouds.

While  $w_B$  (blue, dashed curve in panel (b)) matches  $w_{max}$  (orange, solid curve) very closely, it is still a small overestimate. This is expected given that a perfect balance between vertical advection and the buoyant forcing is an idealisation, with diffusion and lateral mixing still playing a part.

Panels (a) and (b) of Figure 5 consider the behaviour of a single, well-chosen cloud plume, which shows close to ideal behaviour. To understand the overall behaviour of clouds better, we consider all clouds in the simulation and calculate the buoyancy integral  $\mathcal{B}$  up to the height  $z_{max}$  at which the profile of  $w_{max}$  within the cloud attains its maximum value. Since we are interested in the upward moving plumes accelerated by buoyancy, we choose those clouds which have  $w_0$  and  $\mathcal{B} > 0$ . The inset to panel (c) of the same figure shows a scatter plot of the  $w_B$  on the x-axis and the maximum velocity  $w_{max}$  for all clouds for the simulation with  $R = 1.5 \text{ K d}^{-1}$ . All points lie near a line of slope unity (dark-dotted line). In the main panel, we present the same data for varying  $R$  - the data are binned into intervals of uniform  $w_B$  and the average  $w_{max}$  for a given bin is plotted. Again, for all  $R$ , the curves almost exactly match with the line of slope unity, with  $w_B$  being a small underestimate of  $w_{max}$  for clouds with smaller  $w_B$  and vice-versa.

We found that larger values of  $w_B$  (and hence  $w_{max}$ ) correspond to taller clouds while the smaller values correspond to clouds with a small vertical extent. The reason that  $w_B$  remains an overestimate for  $w_{max}$  in taller clouds has

been discussed above. For smaller clouds, we hypothesize that the underestimate comes from smaller clouds which develop close to the lower boundary and are accelerated upward by low-level horizontal convergence.

Overall, the above results remain broadly consistent with our hypothesis that in individual cloud plumes, it is small-scale temperature perturbations and anomalies that exclusively drive the dynamics of the plume, with minimum impact from the large-scales. This is true not only of velocity extremes over the whole run, but also the velocity extreme in each cloud plume.

### 3.2.4 | Deviations from a Moist-Adiabat

In previous sections, we saw that the changes in vertical velocities in updraughts were small, and showed quantitative agreement with buoyancy integrals. However, estimating these buoyancy integrals requires the knowledge of maximum temperatures or high temperature percentiles in addition to the average temperature profile. Further, we have seen above that for a ten-fold increase in  $R$ , the average vertical velocity in clouds and the vertical velocity of the fastest rising parcels show a slow increase even as the area of the domain showing moist convection increases with  $R$ . The main impact of the variation in  $R$  is the change in the temperature profile - the domain becomes colder for larger  $R$ . Since we calculate the temperature profile of a moist-adiabatic ascent from the surface where the surface temperature and moisture boundary conditions do not change, the theoretical moist-adiabatic profile stays fixed for varying  $R$ . This cooling of the domain thus leads to an increase in CAPE.

Unlike CRM simulations, where surface fluxes are parameterised using bulk formulas, our simulations develop a dissipative boundary layer where  $T$  and  $q$  decrease steeply. Calculation of CAPE assumes ascent along a dry adiabat from the surface up to the LCL, followed by ascent along a moist-adiabat. In our case, instead of following a dry adiabat to the LCL, surface parcels are strongly affected by diffusion, as the diffusive boundary layer covers a significant fraction of the sub cloud layer ( $\sim 50\%$ ) and the lapse rate in this layer is significantly steeper than the dry adiabatic one. The gradients in the diffusive layer also become steeper with increasing  $R$  in accordance with equation (11). Attempts to construct modified moist-adiabatic ascents using the domain average temperature profile from above the dissipative layer, for example starting from the height of lowest cloud formation from the simulation or from the height at which the domain-mean temperature first reaches the dew point corresponding to  $q_{bot}$  also yield poor predictions of  $w_{max}$  for varying  $R$ .

Here, we attempt to improve our quantitative estimates of maximum velocity based on a theoretical estimate of CAPE which accounts for entrainment, which is the mixing of non-cloudy, drier and colder air from the environment into cloud plumes. Entrainment is an important process in the ascent of cloud plumes, one that we expect to play a significant role in our case where the temperature of the environmental air varies significantly with variation in  $R$ . We thus further investigate the changes in vertical velocities in light of recent theoretical developments on what sets the strength of updraughts [24, 22].

Singh and O'Gorman [24] introduced a model to quantify the effect of entrainment on undilute ascent. The model assumes an environmental temperature profile in equilibrium with an entraining plume with an entrainment rate of  $\epsilon \text{ km}^{-1}$ . The temperature difference between the environment and the undilute plume, denoted  $\Delta T_u$ , for our model is then given by

$$\frac{\partial}{\partial z} (\Delta T_u) = \frac{\epsilon L_v}{1 + \alpha L_v q_s(\bar{T})} (1 - R_e) q_s(\bar{T}), \quad (22)$$

where  $R_e$  is the horizontal domain average relative humidity and  $\bar{T}$  is the average temperature at a given height



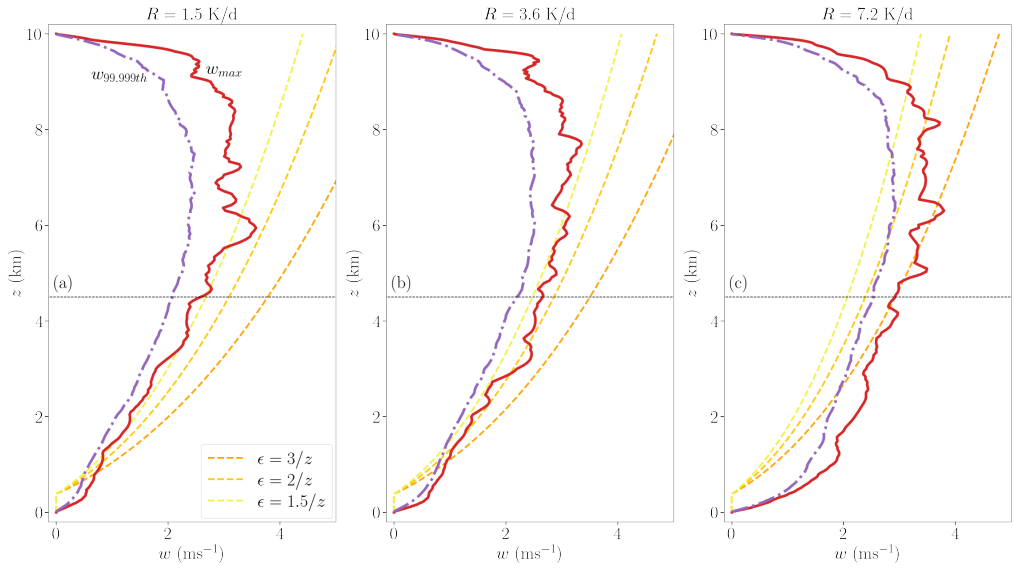


**FIGURE 6** Maximum (red, solid curve) and 99.999th percentile vertical velocity at each height for the entire simulation run compared to the estimated vertical velocity from the buoyancy integral for a parcel with temperature anomaly given by equation (22) with three different entrainment rates  $\epsilon$  for (a)  $R = 1.5 \text{ K d}^{-1}$ , (b)  $R = 3.6 \text{ K d}^{-1}$  and (c)  $R = 7.2 \text{ K d}^{-1}$ .

$z$ . Using fixed  $R_e = 0.4$  (typical value in bulk of the domain for all  $R$ ) and assuming entrainment to be inversely proportional to height [25], we estimate  $\Delta T_u$ , starting the integration from the theoretical LCL for the given boundary conditions ( $z = 0.404 \text{ km}$ ). The actual height of first instance of condensation remains below 500m in the simulations for all  $R$ . The estimate of  $\Delta T_u$  leads to a prediction for  $w_{max}$  via the buoyancy integral. This approach has the added advantage that it requires only an estimation of the domain-averaged temperature profile and not any other measurements from the simulations, such as the high-percentile temperature values.

Figure 6 shows the predicted velocity using the temperature of the undilute plume ascent for 3 different values of  $\epsilon$  for 3 values of  $R$ . The predicted velocity is 0 until the height of the LCL, following which it increases to match very closely  $w_{max}$  between  $z \sim 3 \text{ km}$  and  $6.5 \text{ km}$ , with the closest matching  $\epsilon$  increasing for increasing  $R$ . Higher entrainment for higher  $R$  flows can be expected from the increased area undergoing convection, which leads to a greater turbulent kinetic energy and mixing and a lower typical distance between plumes, which leads to the interplume region being less quiescent. The domain-average turbulent kinetic energy ( $\langle |u|^2/2 \rangle$ ) shows a super-linear increase with increasing  $R$  and specially for the two largest values of  $R$  studied, several rising plumes are present in the domain at all times (for example, see lower panel of Figure 2). If we assume as given that an entraining plume sets the environmental temperature, the above results can be understood as an estimate for the degree of entrainment in clouds in the simulations, with enhanced entrainment arising for larger  $R$ .

### 3.2.5 | Comparison with Dry Convection

Finally, to understand the effect of moisture, we compare the moist simulations with their corresponding dry simulations, which are run with all parameters identical except  $L_v$ , which is set to zero, so moisture is now a passive tracer

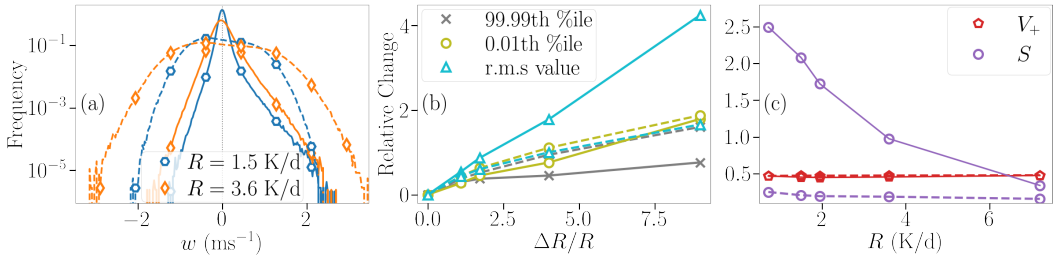


**FIGURE 7** Figure showing comparison of the statistics of vertical velocity  $w$  measured at height  $z = 4.5$  km for moist simulations (solid lines) and dry simulations (dashed lines). (a) Normalised log-histogram of simulations for two different values of  $R$  (see legend). Dotted gray vertical line shows  $w = 0$ . (b) Relative change in the value of the 99.99th percentile, 0.01th percentile and the root mean square value of  $w$  plotted against relative change in  $R$ . (c) The fraction  $V_+$  of grid points with  $w > 0$  and the skewness plotted against  $R$ .

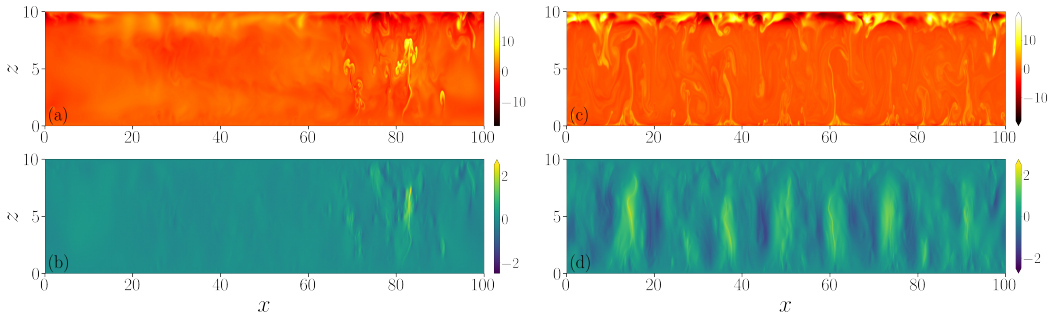


**FIGURE 8** Instantaneous snapshots of the height-wise temperature anomaly (top panels) and vertical velocity (lower panels) for dry simulations (left panels) and moist simulations (right panels) for the case of  $R = 1.5$  K d<sup>-1</sup>.

without any impact on the dynamics. Uniformly cooled dry convection, known as the Prandtl system, is a well-studied system in fluid dynamics literature and finds several applications in the study of the atmospheric boundary layer (see Chapter 3 of [26]). The large-scale balances given by equations (11) and (12) are still valid, with the moisture terms dropping out of the equations.

Panel (a) of Figure 7 shows the histogram of the vertical velocity for values of  $R$  for the dry case (dashed lines) as well as the moist case (solid lines). Both histograms peak to the left of  $w = 0$ , with the median velocity being negative (downward). The distributions of the dry systems are flatter near  $w = 0$ , with the tails of the distribution being nearly symmetric. We note in passing that the dry case without radiative cooling has an up-down symmetry ( $T \leftarrow -T, z \leftarrow -z$ ), and interior cooling breaks this symmetry [20, 21]. The moist distributions on the other hand are more sharply peaked, with broad tails. The asymmetry is also more pronounced, with the positive tail of the moist distribution being broader than the negative tail. Physically, this additional up-down asymmetry in the moist case comes from precipitation. Upward convection is associated with condensation and concomitant release of latent heat, thus occurring on a moist adiabat. But since all condensates are assumed to instantaneously precipitate in our simple model, the downward convection does not contain condensates nor the corresponding latent cooling from evaporation, and instead occurs on a dry adiabat. Note that the up-down asymmetry in moist convection is also

consistent with energetic arguments, even in the absence of interior radiative cooling [27]<sup>1</sup>.

Variation in  $R$  also impacts the histograms. Increasing  $R$  increases the overall convection in the domain, as measured by the convective heat-flux  $\overline{wT}$ , leading to larger kinetic energy and faster velocities on average. This is seen as a flattening of the distribution of  $w$  and a shift of the median  $w$  slightly to the left. It is worth noting that in the dry case, both the positive and the negative ends of the distribution shift outward for an increase in the magnitude of  $R$ . However, in the moist case only the negative end of the distribution shifts significantly, the positive extrema remain nearly fixed - this phenomenon in the moist case has been discussed in detail in the previous sections. We can quantify the shift in the distribution by looking at their relative changes. Panel (b) of the same figure shows the relative change in the 0.01th percentile, 99.99th percentile and the root mean square (r.m.s) value of  $w$  at a fixed height for dry and moist simulations.

Indeed we see that in the dry cases (dashed lines), increasing  $R$  leads to a proportional increase in the fastest updraughts (99.99th percentile) and the fastest downdrafts (0.01th percentile) along with an increase in the typical magnitude of  $w$  as measured by its r.m.s value. The subsiding branch of the moist distribution behaves similar to the dry distribution, while the r.m.s value shows a large increase compared to the dry simulations.

Finally, in panel (c) we study the fraction  $V_+$  of the domain which has  $w$  positive (red curves). We emphasise here that the area fraction  $V_+$  is different from the cloudy area fraction  $\sigma$  discussed in earlier sections - the latter is a feature of moist convection alone and is closely associated with moist convective plumes.  $V_+$  on the other hand includes any point in the domain that is instantaneously moving upward, even far away from clouds or convective plumes, which could be caused either by turbulent fluctuations or gravity waves. Such upward motion does not necessarily lead to condensation. For both moist and dry simulations,  $V_+$  lies just below 0.5. This asymmetry has been studied previously (see [21]), wherein highly convective, turbulent flows have nearly half of the domain moving upward even in the presence of a strong up-down asymmetry. A better measure of the asymmetry is the skewness measure  $S$ , also shown in panel (c) (purple curves). The skewness of the dry and the moist simulations decrease with increasing magnitude of  $R$ . However, the skewness in the moist case is far higher, indicating a greater degree of asymmetry in the dynamics.

While in both cases, the net heat transfer is identical and is set by the large-scale balances with  $R$ , in the moist case, the transport of moisture also contributes to the heat-transfer by latent-heating. A moist updraught simultaneously transports sensible heat and latent heat upward. For this reason, the dry systems have a larger kinetic energy and need to have more net convection, either by area or intensity. Figure 8 shows instantaneous temperature and vertical velocity snapshots of moist convection (left panels) and dry convection (right panels). The moist case shows one strong rising hot, moist plume and a broad region of subsidence outside this plume, whereas the dry convection has an equal number of rising and subsiding, coherent plumes respectively. The largest  $R$  that has been investigated in this study shows similar statistics for both dry and moist convection - indeed in the limit of very large  $R$ , we predict that the domain would be cold enough that moist processes are negligible and the system would converge to the dynamics of dry convection.

## 4 | CONCLUSION AND DISCUSSION

We have presented here a study of Rainy-Bénard convection, introduced by Vallis et. al. [13], in line with several similar models that have been studied before by others. We run simulations for realistic fixed boundary temperature

<sup>1</sup>This excellent paper can be found in pages 11 - 16 of the PDF document titled 'Proceedings at the meetings of the society. January 19, 1938' from Volume 64, Issue 275 available for download from the online archives of the journal.

and moisture boundary conditions on a 2D domain with aspect ratio 10 and vary the radiative cooling  $R$ . We analyse and present the results for 5 different values of  $R$ . The boundary conditions and parameters are chosen such that in the absence of radiative cooling, the system is conditionally unstable to moisture, i.e. the dry system is stable while the moist system is unstable without steady-convection. For the smallest value of (non-zero)  $R$  studied here, the dry system is already unstable to convection while the moist system shows steady-convection. Thus, the parameters chosen are such that the system is destabilised simultaneously by both moisture as well as the bulk radiative cooling.

We characterise the changing behaviour of the system for varying  $R$ , in particular the change in the time-averaged profiles of the prognostic variables temperature and specific humidity. In line with previous studies which used Cloud Resolving Models, we find in our simplified model that the intensity of convection, measured by the average upward velocity in clouds, increases much slower than  $R$ , while the cloudy area fraction, measured as the fraction of points having relative humidity  $q/q_s > 0.98$ , increases as fast as  $R$ . The corresponding increase in cloudy mass flux (vertical velocity times cloudy area) can be related through mass conservation to increased subsidence velocity. The average subsidence velocity outside clouds increases with increasing  $R$ , with a magnitude closely following the theoretical prediction from the heat equation in the absence of condensation. This leads to the cloudy mass flux increasing approximately linearly with  $R$  (albeit slightly faster due to decreased  $(\Gamma_d - \Gamma_m)$ , § 3.2.1), with the increase being dominated by the increase in cloudy areas of the domain.

We also investigate the maximum vertical velocity in the simulations for different  $R$ , finding that the upward velocity extremes remain nearly constant, with an increase even slower than the average velocity in clouds. This was compared to the Convective Available Potential Energy and it was found that the prediction from CAPE was an overestimation, with CAPE increasing uniformly with increasing  $R$  while  $w_{max}$  remained fixed. The buoyancy integrals of the extreme temperatures were instead found to closely predict the extreme vertical velocities, consistent with earlier findings in CRMs [11, 24]. Extreme vertical velocities within individual cloud plumes were also found to be closely related to the buoyancy integral of the extreme temperature anomaly within the same cloud, showing that the mechanism holds even for a single plume and not only as a large-scale statistic.

The physical factors that set the maximum temperature remains an open question. In the study we provide one possible explanation based on the ascent of an undilute plume in an environment set by an entraining plume model, following and adapting ideas introduced by Singh and O’Gorman [24]. Importantly, regardless of the buoyancy estimate used for  $w$  in updraughts, all change only weakly with  $R$ , providing constraints from convective physics that limits the increase in  $w$  and explains why the convective mass flux increase is almost entirely reached through increased cloud area.

Finally, we compare the behaviour of the moist model to the corresponding dry simulations, which sheds light on the degree of up-down asymmetry inherent in the system. Both, the  $-R$  term in the equations and the asymmetry between condensation and evaporation leads to an up-down asymmetry. We find here that while the dry simulations with radiative cooling are well into the turbulent convective regime and have only a small degree of up-down asymmetry in the vertical velocity, as measured by the frequency of rising parcels of fluid or the skewness of the vertical velocity, the moist simulations show a larger degree of up-down asymmetry for all  $R$ , with the behaviour of the moist system converging towards dry convection at the largest  $R$ .

The main drawbacks of using idealised models with Direct Numerical Simulation as an atmospheric model is the requirement of very fine resolution grids to have realistic values of molecular diffusivity and conductivity. In the absence of such high resolution or parametrisation of sub-grid fluxes, we are forced to set  $\kappa$  and  $\nu$  to unrealistically large values, with the most immediate effect being the presence of a diffusive boundary layer ( $\sim 200$  m high) which is far larger than the atmospheric skin layer (usually few metres thick). This impacts the relative humidity and temperature profile in the convective bulk, leading to measured values in the simulations that can differ from the true atmospheric

values. Comparison with more complex CRMs and finer resolution direct numerical simulations is desirable to further investigate the role of boundary layers and surface fluxes. We still find that our 2D idealised model shows realistic behaviour in its response to changing  $R$  and various convective processes. Further, we have shown how such a simple model can be a good test-bed for performing analysis on atmospheric models with simplified dynamics and offers fundamental insights into the atmospheric system, such as the degree of the asymmetry and the estimation of entrainment. Further, simple models can be used as a starting point in the analysis of basic fluid instabilities.

Future avenues of investigation which retain the simplicity and the ease of implementation of the current approach include the response of the system to varying boundary conditions and changing fluid parameters, such as  $\beta$ ,  $\nu$ ,  $\kappa$  to more realistic values by employing higher resolution. Further, the first-order dynamic effects of non constant radiative cooling can also be investigated using the current model - for example varying the  $R$  parameter as a function of whether the grid point is cloudy ( $q > q_s$ ) or not cloudy. While here we emphasise the possible direct applications to the study of moist convection as an alternative to CRMs and other more sophisticated models, the current model by itself is of broad interest to researchers studying fundamental fluid dynamics and instabilities, chaos, turbulence and dynamic systems in general. The system is particularly rich in transitions and dynamics given that the dynamics of the system itself feeds back on to the energetics of the system - moisture provides a feedback between convection and energy as more convection leads to more latent-heating, thus more buoyant forcing and convection. However, latent-heating aloft also stabilises the system by increasing the temperature of the bulk and decreasing the effective Rayleigh number. We believe that such simplified approaches can help improve our fundamental understanding of the complex behavior of moist convection.

## Acknowledgements

The authors gratefully acknowledge the help of Julian Renaud and Alzbeta "Bety" Pechacova. Julian went through the relevant literature on the topic in the initial stages of the study in a very thorough manner and allowed the authors to understand the various types of idealised models that have been studied and the various approaches used. Bety ran simulations and performed analysis of the outputs of several simulations, which were crucial to bringing the article to its final form.

The authors also acknowledge the input of Prof. Martin Singh (Monash University, Australia) and discussions with Gregory Dritschel, Prof. Steven Tobias and Prof. Douglas Parker (Leeds University, United Kingdom).

This project has received funding from the European Union's Horizon 2020 research and innovation programme under the Marie Skłodowska-Curie grant agreement No. 101034413. CM gratefully acknowledges funding from the European Research Council (ERC) under the European Union's Horizon 2020 research and innovation program (Project CLUSTER, Grant Agreement No. 805041). This research was supported by the Scientific Service Units (SSU) of IST Austria through resources provided by Scientific Computing (SciComp).

## conflict of interest

You may be asked to provide a conflict of interest statement during the submission process. Please check the journal's author guidelines for details on what to include in this section. Please ensure you liaise with all co-authors to confirm agreement with the final statement.

## references

- [1] Jeevanjee N, Fueglistaler S. Simple spectral models for atmospheric radiative cooling. *Journal of the Atmospheric Sciences* 2020;77(2):479–497.
- [2] Manabe S, Strickler RF. Thermal equilibrium of the atmosphere with a convective adjustment. *Journal of the Atmospheric Sciences* 1964;21(4):361–385.
- [3] Tompkins AM, Craig GC. Radiative–convective equilibrium in a three-dimensional cloud-ensemble model. *Quarterly Journal of the Royal Meteorological Society* 1998;124(550):2073–2097.
- [4] Eyring V, Bony S, Meehl G, Senior C, Stevens B, Stouffer R, et al. Overview of the Coupled Model Intercomparison Project Phase 6 (CMIP6) experimental design and organisation. *Geoscientific Model Development Discussions* 2015;8(12).
- [5] Khairoutdinov MF, Randall DA. Cloud resolving modeling of the ARM summer 1997 IOP: Model formulation, results, uncertainties, and sensitivities. *Journal of the Atmospheric Sciences* 2003;60(4):607–625.
- [6] Arakawa A, Wu CM. A unified representation of deep moist convection in numerical modeling of the atmosphere. Part I. *Journal of the Atmospheric Sciences* 2013;70(7):1977–1992.
- [7] Klein SA, Hall A, Norris JR, Pincus R. Low-cloud feedbacks from cloud-controlling factors: A review. *Shallow clouds, water vapor, circulation, and climate sensitivity* 2018;p. 135–157.
- [8] Bony S, Dufresne JL. Marine boundary layer clouds at the heart of tropical cloud feedback uncertainties in climate models. *Geophysical Research Letters* 2005;32(20). <https://agupubs.onlinelibrary.wiley.com/doi/abs/10.1029/2005GL023851>.
- [9] Zelinka MD, Klein SA, Qin Y, Myers TA. Evaluating climate models' cloud feedbacks against expert judgment. *Journal of Geophysical Research: Atmospheres* 2022;127(2):e2021JD035198.
- [10] Khairoutdinov M, Randall D, DeMott C. Simulations of the atmospheric general circulation using a cloud-resolving model as a superparameterization of physical processes. *Journal of the Atmospheric Sciences* 2005;62(7):2136–2154.
- [11] Muller CJ, O’Gorman PA, Back LE. Intensification of precipitation extremes with warming in a cloud-resolving model. *Journal of Climate* 2011;24(11):2784–2800.
- [12] Singh MS, O’Gorman PA. Influence of microphysics on the scaling of precipitation extremes with temperature. *Geophysical Research Letters* 2014;41(16):6037–6044. <https://agupubs.onlinelibrary.wiley.com/doi/abs/10.1002/2014GL061222>.
- [13] Vallis GK, Parker DJ, Tobias SM. A simple system for moist convection: the Rainy–Bénard model. *Journal of Fluid Mechanics* 2019;862:162–199.
- [14] Hernandez-Duenas G, Majda AJ, Smith LM, Stechmann SN. Minimal models for precipitating turbulent convection. *Journal of Fluid Mechanics* 2013;717:576–611.
- [15] Pauluis O, Schumacher J. Idealized moist Rayleigh–Bénard convection with piecewise linear equation of state. *Communications in Mathematical Sciences* 2010;8(1):295–319.
- [16] Ahlers G, Grossmann S, Lohse D. Heat transfer and large scale dynamics in turbulent Rayleigh–Bénard convection. *Reviews of modern physics* 2009;81(2):503.
- [17] Robe FR, Emanuel KA. Moist convective scaling: Some inferences from three-dimensional cloud ensemble simulations. *Journal of Atmospheric Sciences* 1996;53(22):3265–3275.
- [18] Burns KJ, Vasil GM, Oishi JS, Lecoanet D, Brown BP. Dedalus: A flexible framework for numerical simulations with spectral methods. *Physical Review Research* 2020;2(2):023068.

- [19] Bretherton CS, Smolarkiewicz PK. Gravity waves, compensating subsidence and detrainment around cumulus clouds. *Journal of Atmospheric Sciences* 1989;46(6):740–759.
- [20] Berlingiero M, Emanuel K, Von Hardenberg J, Provenzale A, Spiegel E. Internally cooled convection: a fillip for Philip. *Communications in Nonlinear Science and Numerical Simulation* 2012;17(5):1998–2007.
- [21] Agasthya L, Muller C, Dynamics and Scaling of Internally Cooled Convection; 2023.
- [22] Singh MS, O’Gorman PA. Increases in moist-convective updraught velocities with warming in radiative-convective equilibrium. *Quarterly Journal of the Royal Meteorological Society* 2015;141(692):2828–2838. <https://rmets.onlinelibrary.wiley.com/doi/abs/10.1002/qj.2567>.
- [23] van der Walt S, Schönberger JL, Nunez-Iglesias J, Boulogne F, Warner JD, Yager N, et al. scikit-image: image processing in Python. *PeerJ* 2014 6;2:e453. <https://doi.org/10.7717/peerj.453>.
- [24] Singh MS, O’Gorman PA. Influence of entrainment on the thermal stratification in simulations of radiative-convective equilibrium. *Geophysical Research Letters* 2013;40(16):4398–4403.
- [25] Holloway CE, Neelin JD. Moisture vertical structure, column water vapor, and tropical deep convection. *Journal of the atmospheric sciences* 2009;66(6):1665–1683.
- [26] Emanuel KA. Atmospheric convection. Oxford University Press, USA; 1994.
- [27] Bjerknes J. Saturated-adiabatic ascent of air through dry-adiabatically descending environment. *QJ Roy Meteor Soc* 1938;64:325–330.